Tungsten and Molybdenum Ablation Modeling for Re-entry Applications

H. L. Moody,* D. H. Smith,* R. L. Haddock,* and S. S. Dunn*
Prototype Development Associates, Inc., Santa Ana, Calif.

Refractory metals are attractive candidates for re-entry vehicle nosetips due to their high resistance to water droplet and ice particle erosion. Ablation models are presented for tungsten, tungsten/25% rhenium, and molybdenum, including gas diffusion-limited thermochemical ablation and liquid phase removal. Chemical equilibrium is assumed in the gas phase with kinetics for tungsten ablation considered only at the ablating surface. These models have been incorporated into computer programs that also include shape change, boundary-layer transition, surface roughness, and two-dimensional transient conduction. Good correlation for high- and low-pressure arcjet tests, ballistic range firings, and sounding rocket flights has been obtained with these models.

Nomenclature

B = normalized thermochemical ablation rate
Ch = Stanton number
H = enthalpy (Ref. at 536°R), Btu/lb
K = thermal conductivity, Btu/ft-sec-°R
K_I, K_{max} = initial and maximum roughness heights, in.
$K(T)$ = equilibrium constant
M = Mach number
$\dot{m}$ = mass loss, lb/ft^2-sec
Mw = molecular weight, lb/lb-mole
n_i = species stoichiometric coefficients
P = pressure, atm
q = convective heat flux, Btu/ft^2-sec
Re_θ = momentum Reynolds number
R_n = nose radius, ft
T = temperature, °R
x = distance below material surface
X_i, X_T = species mole number and total gas moles
Z_i = chemical constituents
$\rho_e U_e$ = boundary-layer edge mass flux, lb/ft^2-sec
Θ = momentum thickness, in.
η = blowing correction factor

Subscripts

B = blowing
c = condensed phase
cw = cold wall
e = boundary-layer edge
g = gas phase
gw = gas wall
I = injectant
ℓw = liquid wall
o = no blowing
r = recovery
rad = radiation
T_2 = stagnation condition
sw = solid wall
w = wall

I. Introduction

AVAILABLE ground and flight test data indicate that conventional re-entry vehicle nosetips experience high recession rates during flight through atmospheric weather (condensed phase) environments. To minimize weather effects on vehicle performance, considerable effort is being devoted throughout industry to minimize nosetip ablation in erosive or particle-laden environments. One candidate erosion-resistant nosetip concept is a composite design consisting of a conventional graphitic external, or primary, nosetip and an erosion-resistant inner nosetip, or subtip. The primary nosetip is designed to survive to impact in clear air re-entry flight, whereas the subtip is provided to assure vehicle survival to impact when the primary nosetip is removed prematurely in an erosive weather environment.

This erosion-resistant nosetip (ERN) concept was developed in the study reported in Ref. 1, which included a material screening test program to evaluate candidate subtip materials. The candidate materials consisted of several state-of-the-art refractory metals, ceramics (in the form of carbides and nitrides), and material composites that were investigated on the basis of thermochemical ablation performance, erosion resistance, and thermostructural performance. The only materials showing satisfactory performance in all three areas were tungsten, tungsten/25% rhenium, and (to a lesser extent) molybdenum.

Analytical ablation models were developed for these three refractory metals for use in nosetip design calculations. In order to evaluate the accuracy of the ablation models, calculations were performed to correlate the results of several ablation tests of these materials in ground test facilities. The tests included: 1) arcjet tests of molybdenum, tungsten and tungsten alloys at model stagnation pressures ranging from 60 to 100 atm; 2) ballistic range tests of tungsten and molybdenum at peak stagnation pressures ranging from 90 to 210 atm; and 3) low-pressure (0.07 atm) arcjet tests of tungsten in test streams of both simulated air and pure nitrogen.

In addition, tungsten nosetips were recovered from two flight tests using sounding rockets. One flight test was performed in clear air and the other in weather. The tungsten ablation model was applied to each flight test and, in each case, excellent agreement was achieved between the predicted and recovered nosetip shape and total recession.

This paper presents the ablation models that were developed for tungsten, tungsten/25% rhenium, and molybdenum, and it summarizes the most significant ground and flight test data correlations that have been made to verify the validity of the analytical models. Additional data correlations are provided in Refs. 2–5.

II. Thermochemical Ablation Models

The thermochemical behavior of the refractory metals in re-entry flight is postulated to involve three principal regimes of ablation: 1) rate- or kinetic-limited formation and vaporization of an oxide layer; 2) diffusion-limited formation

Presented as Paper 75-112 at the AIAA 13th Aerospace Sciences Meeting, Pasadena, Calif., Jan. 20-22, 1975; submitted July 8, 1976; revision received Sept. 17, 1976. This work was performed under Defense Nuclear Agency Contract DNA 001-74-C-003.

Index categories: Material Ablation; Thermochemistry and Chemical Kinetics.

*Engineering Associate.

of a condensed oxide, with material removal in the form of oxide vaporization and oxide melt runoff; and 3) diffusion-limited vaporization and oxidation of tungsten in the vapor phase, and melt runoff of the parent material. Thermochemical ablation is modeled using the thermochemical ablation potential, B, as derived by Dension.[6] Material removal by melt runoff of the parent metal and condensed metal oxides is estimated from surface heat and mass balances, assuming that the liquid layer is removed instantaneously (i.e., zero liquid thickness).

Tungsten

Thermochemical modeling in the diffusion-limited regimes was accomplished by assuming thermochemical equilibrium and utilizing the thermochemical ablation potential defined as

$$B=\dot{m}_g/\rho_e U_e C h_B \tag{1}$$

where B is the amount of surface material required chemically to saturate one unit mass of freestream gas. With this, the thermochemical ablation rate of tungsten in air is expressed by

$$\frac{B}{184}W+\frac{0.233}{32}O_2+\frac{0.767}{28}N_2 \rightarrow X_O+X_{O_2}+X_{NO}+X_{N_2}$$
$$+X_W+X_{WO}+X_{WO_2}+X_{WO_3}+X_{W_2O_6}+X_{W_3O_9}$$
$$+X_{W_3O_8}+X_{W_4O_{12}}+X_{WO_3}{}^*+X_{WO_2}{}^* \tag{2}$$

where the asterisk (*) denotes condensed species. The gaseous species mole numbers, X_i, are related to temperature and pressure by the mass action law

$$\Pi_i X_i^{n_i}=(P/X_T)^{-\Sigma n_i}K(T) \tag{3}$$

which is written for a reaction with stoichiometric coefficients, n_i, of the form

$$\Sigma n_i Z_i=0 \tag{4}$$

By applying species conservation principles in Eq. (2) to oxygen, nitrogen, and tungsten, and by observing the fact that the free energy of the reactants must be minimized, the equations can be solved for the thermochemical potential, B, and the species mole numbers, X_i. The preceding chemical reactions and principles were added to the computer code described in Ref. 7. The revised code was used to model refractory metal oxidation. The species thermodynamic properties were obtained from JANAF.[8]

The thermochemical ablation potential, gas-wall enthalpy, and molecular weight of the boundary-layer injectants for tungsten are presented in Figs. 1 and 2. The ablation potential of Fig. 1, as defined in Eq. (1), represents mass removal in the form of both gaseous and condensed oxide species. The transition from condensed oxide-gas phase mass loss to all gas phase mass loss is noted in Fig. 1 as a function of pressure. At temperatures below the noted transition points, that portion of the mass removed in the form of condensed oxides, WO_3^* and WO_2^*, is represented by the area noted in Fig. 1.

From the investigations of Perkins,[9] the oxides are relatively stable at temperatures below approximately 2300°R, and tungsten mass loss is almost nonexistent. At temperatures above 2300°R, tungsten mass loss can be influenced by surface kinetics, and the kinetic-limited ablation rates of Perkins have been adopted.[5] Transition from kinetic- to diffusion-limited ablation is characterized by the intersection of the kinetic nondimensional ablation rate with the curves of Fig. 1.

The ablation performance of the material is determined by coupling the thermochemical process to a solution for subsurface heat conduction. This coupling is via heat and mass

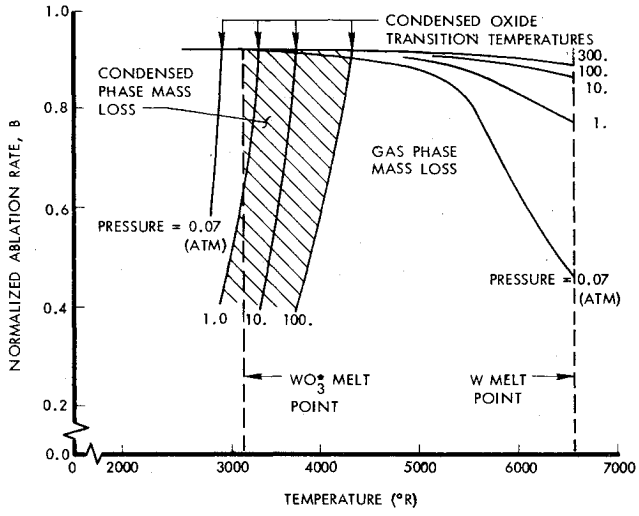

Fig. 1 Thermochemical ablation of tungsten in air.

balances applied to a control volume as shown in Fig. 3.

At temperatures below the melting point of tungsten, 6570°R, the surface heat balance is

$$-K\mathrm{d}T/\mathrm{d}x\Big|_{x=0}=\rho_e U_e C h_B(H_r-H_{gw})+\dot{m}_w H_{sw}$$
$$-\dot{m}_g H_{gw}-\dot{m}_c H_{lw}-q_{\mathrm{rad}} \tag{5}$$

The conduction term

$$-K\mathrm{d}T/\mathrm{d}x\Big|_{x=0}$$

is used in the subsurface conduction solution to compute material temperature response.

At the melting point of tungsten, the amount of ablation due to melt runoff is approximated by fixing the surface temperature at the melt point and assuming the melt layer is infinitesimally thin. Melt runoff is then

$$\dot{m}_c=\left[\rho_e U_e C h_B(H_r-H_{gw})+\dot{m}_g(H_{sw}-H_{gw})\right.$$
$$\left.-q_{\mathrm{rad}}-\left(-K\mathrm{d}T/\mathrm{d}x\Big|_{x=0}\right)\right]\Big/\left(H_{lw}-H_{sw}\right) \tag{6}$$

where

$$-K\mathrm{d}T/\mathrm{d}x\Big|_{x=0}$$

is determined from the subsurface conduction solution.

The change in convective heating caused by the injection of gaseous reaction products into the boundary layer is modeled by the expressions developed by Arne[10] to account for differences in injectant and boundary-layer edge species molecular weight. The expressions are

$$Ch_B/Ch_0=1-\eta\dot{m}_g/\rho_e U_e Ch_0 \tag{7}$$

where for laminar flow

$$\eta=0.68(Mw_w/Mw_I)^{0.4}-0.08(Mw_w/Mw_I)^{0.4}$$
$$\times(\dot{m}_g/\rho_e U_e Ch_0) \tag{8}$$

and for turbulent flow

$$\eta=0.36(Mw_w/Mw_I)^{0.8} \tag{9}$$

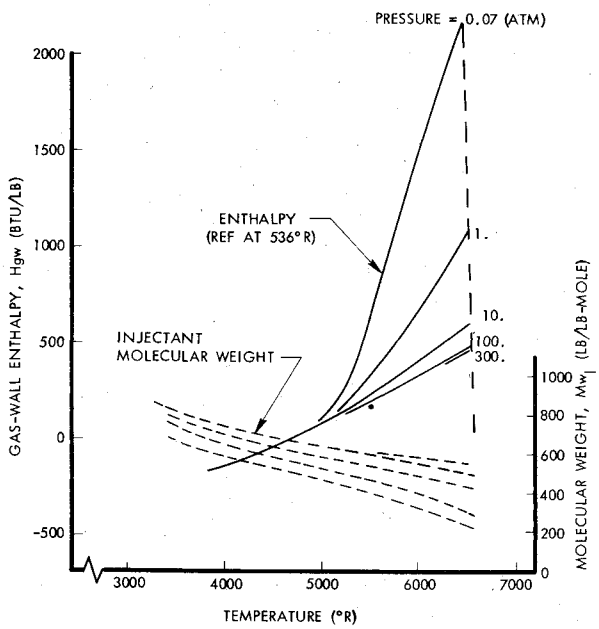

Fig. 2 Enthalpy and molecular weight for tungsten in air.

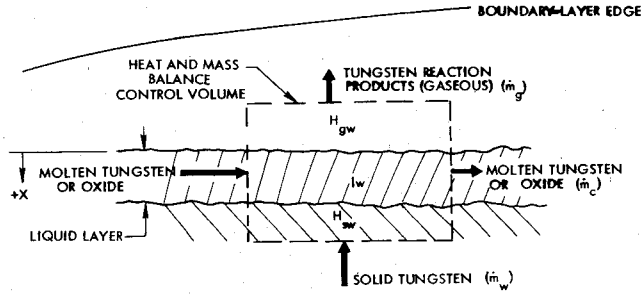

Fig. 3 Schematic.

Molybdenum

The thermochemical ablation of molybdenum was modeled using the same techniques that were used for tungsten. The air reaction products indentified in Eq. (2) and the molybdenum species: Mo, MoO, MoO_2, MoO_3, and MoO_3^* were used in the equilibrium calculations.[11] The species thermochemical ablation potential and gas-wall enthalpy for molybdenum in air are presented in Fig. 4. The species MoO_2^* was not included in the thermochemical calculation because of insufficient thermochemical property data. As was the case for tungsten, there is an ablation regime for which melt runoff of a condensed oxide, MoO_3^*, is likely to occur.

Tungsten/25% Rhenium

The thermochemical ablation of tungsten/25% rhenium was modeled by including the species Re, ReO, ReO_2, ReO_3, Re_2O_7, ReO_2^*, and ReO_3^* in Eq. (2). The data for these species were obtained from Margrave.[12] The thermochemical ablation potentials and gas-wall enthalpies at the melt temperature are presented in Table 1 as a function of pressure.

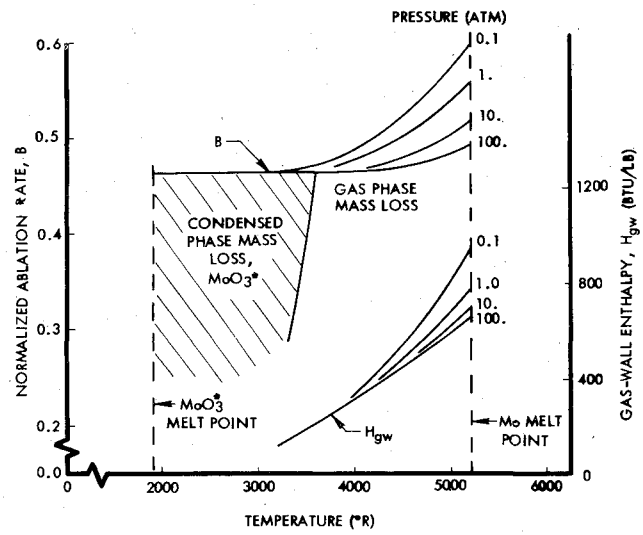

Fig. 4 Thermochemical ablation and enthalpy of molybdenum in air.

Conduction/Shape Change Codes

All of the two-dimensional analyses discussed in this paper were performed with the nosetip shape change erosion and conduction (NOSEC) code which computes the flowfield, heat transfer, ablation, and internal heat conduction histories for noncharring nosetip materials in hypersonic flight. One-dimensional calculations were performed with the PDA ablation, conduction, and erosion (PACE) code. All flowfield and heat transfer parameters in the NOSEC code are solved by a numerical integration along the body in the streamwise direction. The effects of the bow shock-generated entropy layer are accounted for by a streamtube mass balance calculation. The surface pressure distribution is defined by a blast wave-imbedded Newtonian technique that has been shown to be valid for a wide range of arbitrary shapes. The surface heat transfer distributions are computed by standard methods and modified to account for the effects of surface roughness on the onset of boundary-layer transition and on heat transfer. The surface roughness can consist of uniformly distributed (sandpaper-type) roughness, or of the larger cross-hatched, or scallop pattern type of roughness. Distributed roughness is assumed to start at an input initial value (K_i) and to grow at a rate equal to 20% of the local recession rate to an input maximum height (K_{max}). The augmented heating caused by distributed roughness is given by the methods of Powars[13] for turbulent flow and the passive advanced nosetip (PANT) model[14] for laminar flow. The formation, growth rate, and heating augmentation associated with scallop patterns are computed with the methods of White and Grabow.[15]

Roughwall boundary-layer transition is defined by

$$Re_\theta = 275\exp[0.134M_e - 0.662\,K_i/\theta] \qquad (10)$$

The NOSEC code computes the ablation rate for any material/gas composition for which the chemical reactions can be defined in the form of enthalpy, chemical ablation potential, and injectant molecular weight. This is coupled

Table 1 Tungsten/25% rhenium ablation parameters at melt temperature, 6111°R

Pressure, atm	Normalized ablation rate, B	Gas-wall enthalpy, Btu/lb	Injectant molecular weight, lb/lb-mole
300.0	0.911	331.0	580.0
100.0	0.911	344.0	570.0
10.0	0.911	395.0	480.0
1.0	0.925	680.0	400.0

Table 2 Refractory metal and metal oxide properties

Temperature-dependent properties

Temperature, °R	Specific heat[8,11] Btu/lb-°R			Thermal conductivity[16] Btu/ft-hr-°R		
	W	*W*/25%Re	Mo	*W*	*W*/25%Re	Mo
500.0	0.031	0.032	0.058	105.0	86.0	78.0
1000.0	0.033	0.034	0.066	83.0	69.0	72.0
2000.0	0.036	0.037	0.071	68.0	56.0	63.0
3000.0	0.040	0.041	0.082	61.0	52.0	56.0
4000.0	0.043	0.044	0.096	57.0	49.0	51.0
5200.0	0.051	0.052	0.141	53.0	46.0	50.0
6110.0	0.068	0.066	...	52.0	45.0	...
6570.0	0.084	...	...	52.0	...	...

Constant properties

Property	*W*	WO_3^*	*W*/25%Re	Mo	MoO_3^*
Density,[16] lb/ft^3	1200.0	447.0	1234.0	639.0	290.0
Melt point,[8,11] °R	6570.0	3140.0	6111.0	5200.0	1930.0
Liquid specific heat,[8] Btu/lb-°R	...	0.14	...	...	0.21
Heat of fusion,[8,11] Btu/lb	82.8	136.0	81.3	125.0	145.0
Liquid enthalpy,[8,11] Btu/lb	360.0	−1162.0	322.0	525.0	−1716.0
Emissivity, estimated	0.4	0.4	0.4	0.4	0.4

with particle erosion, including shock layer-induced particle deceleration, deflection, and mass loss. The external surface is defined by a series of discrete points that are assumed to recede normal to the instantaneous local slope to define a new profile at the end of each compute interval. Internal temperature distributions are computed by means of a two-dimensional nodal network. The conduction solution (explicit forward difference), surface profile, surface heating and recession calculations are coupled completely.

Material Properties Data

The thermosphysical properties of the refractory metals and the condensed oxides (identified in Figs. 1 and 4) are presented in Table 2. The sources from which the data were acquired are included in the table.

III. Ground Test Correlations

Three groups of ground test ablation programs have been used in the data correlations presented herein. The ground tests were selected to encompass the range of heating conditions encountered in re-entry. The tests, facilities, major test uncertainties, and the data correlations are discussed in the following paragraphs.

Low Pressure Arcjet

Low pressure tungsten ablation tests were conducted in the Aerotherm/Acurex arc plasma generator. The tests were performed using the supersonic anode configuration which produces a nearly uniform 2.0-in. diam test stream from a 3.5-in. exit diam, Mach 3+ nozzle. To isolate the effects of oxidation, tungsten was tested in both simulated air and pure nitrogen. The models were sphere-cylinders with an initial nose radius of 0.25-in. and were made from commercially pure tungsten.

Model ablation and shape histories were obtained during the tests from motion picture coverage at 100 frames/sec. Stagnation point heat flux was obtained for each test condition using a copper slug calorimeter positioned in the center of a 1.25-in. diam, flat-faced model with a 0.125-in. corner radius. The stagnation point pressure was obtained from a 0.375-in. diam pitot probe. The recovery enthalpy of the test stream was computed from the measured heat flux and pressure by

$$q_{cw}\sqrt{R_n} = 0.041\sqrt{P_{T_2}}H_r \qquad (11)$$

The data and details of the tests are presented in Ref. 2. During the tests, all of the models changed from the initial spherical shape to flat-faced cylinders with considerable melt runoff separating off the corner of the model and flowing into the gas stream, Fig. 5. No sidewall recession occurred on any model. The nature of the liquid layer runoff indicated that flow separation occurred at the model edge, resulting in very little sidewall heating.

The comparisons between the predicted and measured stagnation point recession histories of tungsten in both air and nitrogen gas streams are shown in Fig. 5. The time to reach the tungsten melt point in air was 1.12 to 1.20 times longer than the time in the nitrogen stream for essentially the same values of model heat flux. Also, the recession rates in air were lower than in the equivalent heat flux nitrogen tests. These results are to be expected because in air there is a reduction in convective transport due to mass injection of the gaseous ablation products. In nitrogen, tungsten is relatively inert. This will cause, relative to air, higher surface heating because there are no gaseous ablation products to reduce convective heating.

High Pressure Arcjet Tests

High pressure arcjet tests were performed in the Air Force Flight Dynamics Laboratory (AFFDL) 50-Mw arcjet facility. The 1.11-in. and 1.38-in. exit diam nozzles were used in the ablation tests of tungsten, molybdenum, and tungsten/25% rhenium. The 1.11-in. nozzle is a parallel flow nozzle producing an exit Mach number of approximately 1.8, while the 1.38-in. nozzle is flared and produces an exit Mach number of approximately 1.75. Tests were performed in the 1.11-in. nozzle at 60, 80, and 100 atm stagnation pressure, and in the 1.38-in. nozzle at 73 atm stagnation pressure.[2,3] All tests were performed with the spiked enthalpy configuration that produces a central core of high enthalpy air shrouded by a lower enthalpy airstream. High-speed cameras (1000 frames/sec) were used to measure model surface recession and shape change.

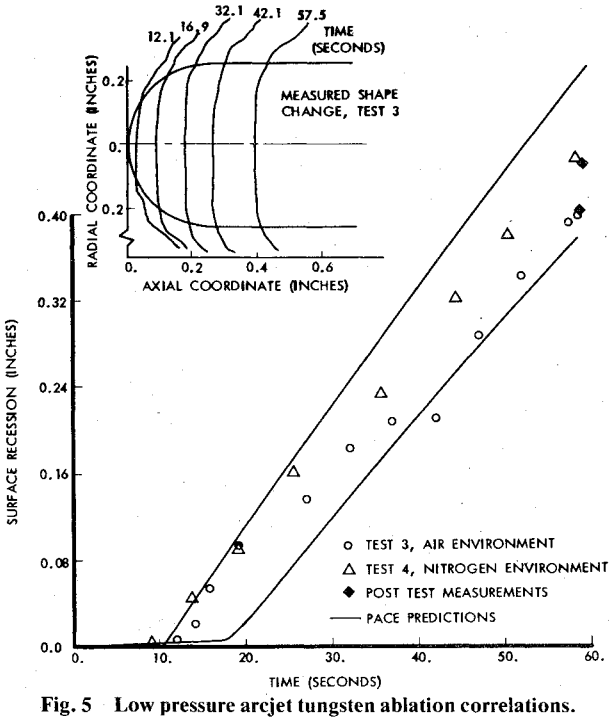

Fig. 5 Low pressure arcjet tungsten ablation correlations.

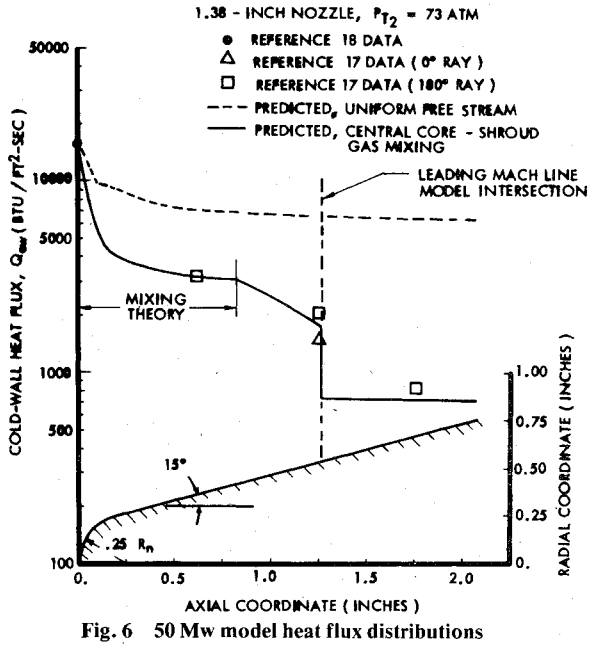

Fig. 6 50 Mw model heat flux distributions

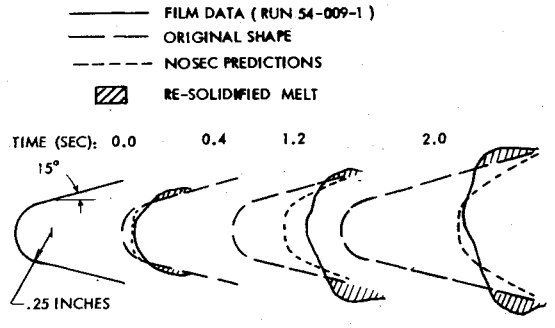

Fig. 7 50 Mw tungsten shape change correlations.

Material ablation predictions in the 50-Mw facility were made using the PACE and NOSEC computer codes. In the NOSEC calculations, heat flux distributions over the model were based upon calorimeter data. These calorimeter data, the predicted heat flux distribution (assuming a uniform freestream), and the heat flux distribution used in the code are presented in Fig. 6. The heat flux measurements were acquired in the 1.38-in. nozzzle using a 0.25-in. nose radius, 15-deg conical calorimeter model.17 The difference between the measured heat flux distribution and those that would exist on a model in a uniform flow environment is postulated to be a consequence of freestream rotational flow characteristics that cause the central core of high enthalpy air to move circumferentially around the model. An analytical technique has been devised to estimate the reductions in recovery enthalpy that occur as a result of the rotational behavior of the flow. The heat flux distribution obtained from the technique is presented in Fig. 6.

The shape change and stagnation point surface recession predicted by the NOSEC code are presented in Figs. 7 and 8, respectively, for the model configuration and heat flux distribution of Fig. 6. The boundary-layer transition criteria and roughwall heating inputs that were used in the predictions are presented in Table 3. Uniformly distributed roughness heating criteria were used in the predictions. The agreement between measured and predicted stagnation point recession is good. A considerable difference, however, exists between the computed and observed shape change histories. A possible explanation for the difference is that the NOSEC code does not calculate melt layers of finite thickness and subsequent melt buildup. In the actual case, a considerable fraction of the melt resolidified on the forward portion of the conical surface (noted in Fig. 7 by the shaded area) causing a blunter shape with lower sidewall heating than was used in the NOSEC code.

A comparison between the NOSEC and PACE code stagnation point recession histories is presented in Fig. 8. The PACE prediction was made using the nose radius histories ob-

Table 3 Boundary-layer transition and roughwall heating criteria

Test facility	Surface roughness height, K (in.)		Minimum transition Reynolds number	Roughwall heating criteria
	Initial	Maximum	Re_θ	
Aerotherm	0.0	0.0	All laminar	None, smooth wall
AFFDL, 50-Mw	0.0003	0.002	40.0	Uniform roughwall.[13] No scallops
AEDC, range G	0.0003	0.002	40.0	Uniform roughwall[13] with transition to scallops[15]
Sounding rocket, clear air	0.0003	0.002	105.0	Uniform roughwall.[13] No scallops
Sounding rocket, weather	0.0003	0.002	105.0	Uniform roughwall[13] with transition to scallops[15]

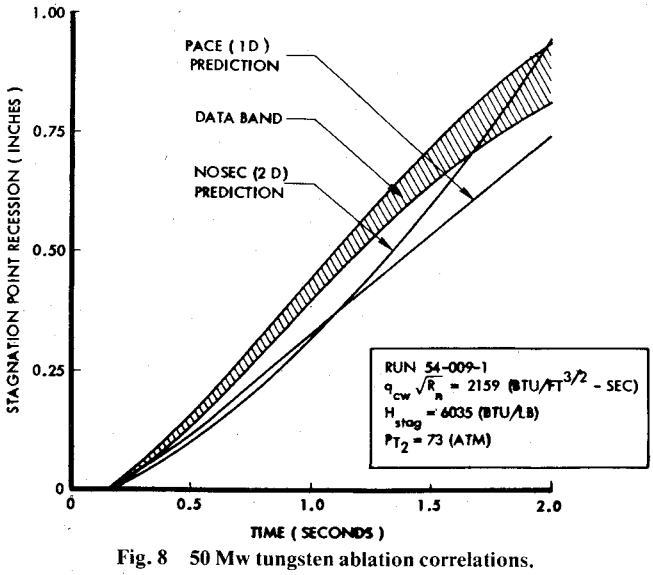

Fig. 8 50 Mw tungsten ablation correlations.

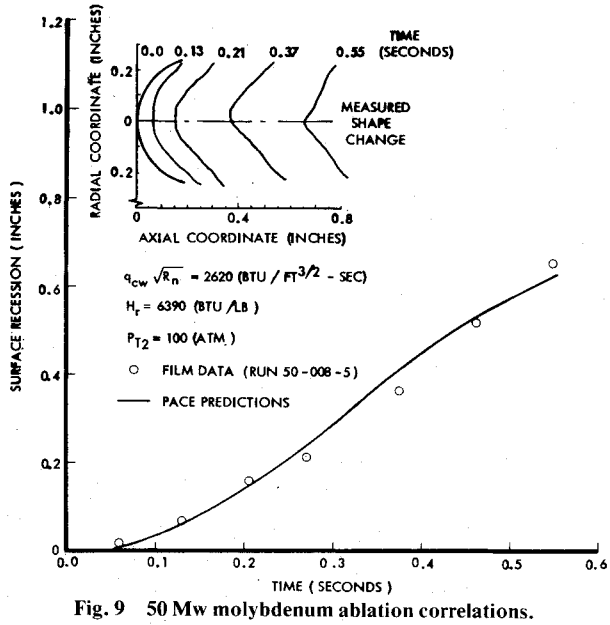

Fig. 9 50 Mw molybdenum ablation correlations.

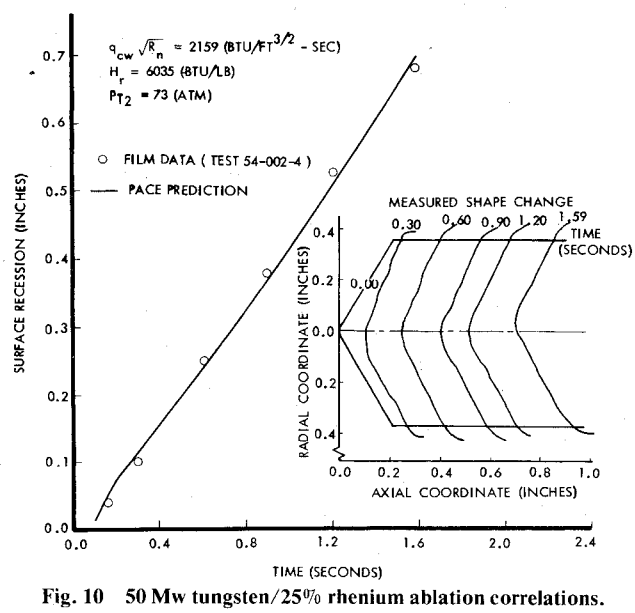

Fig. 10 50 Mw tungsten/25% rhenium ablation correlations.

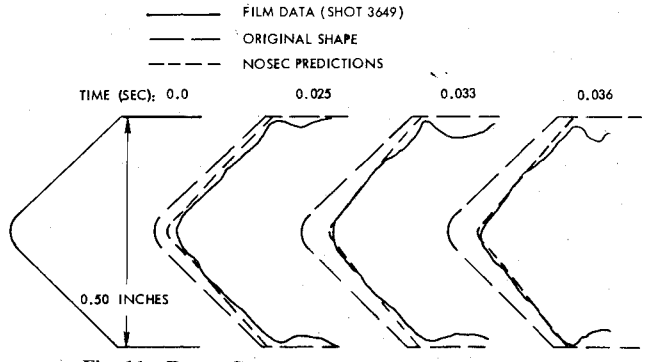

Fig. 11 Range G tungsten shape change correlations.

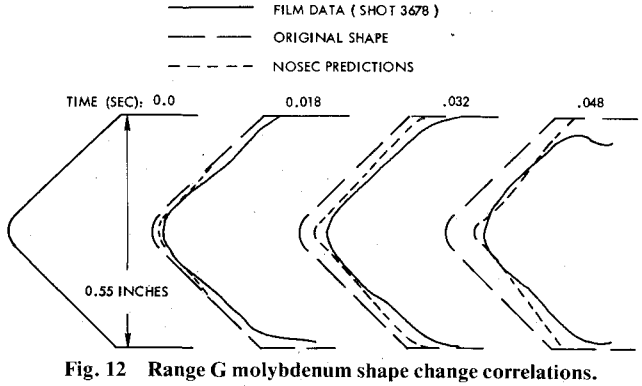

Fig. 12 Range G molybdenum shape change correlations.

served in the test and the heating parameter $q_{cw}(R_n)^{1/2}$ as reported in Ref. 18. While there is reason to believe that the heating in the 50-Mw does not scale by $1/(R_n)^{1/2}$, and that two-dimensional conduction should be included in the data correlations, the agreement between the one-dimensional and two-dimensional predictions and the observed ablation history is nevertheless good. Based upon this correlation, the more cost effective PACE code was used for most of the 50-Mw data correlations.[2,3]

Comparisons between the predicted and measured stagnation point recession histories of the molybdenum and tungsten/25% rhenium models are presented in Figs. 9 and 10, respectively. In each case, the predictions were made with the PACE code using convective heating histories that were corrected for the observed nose radius histories.

Ballistic Range Tests

The Arnold Engineering Development Center (AEDC) Range G consists of a hypervelocity gun and approximately 850 ft of instrumented range in which ambient pressure can be adjusted to any desired level from near zero to one atmosphere. The primary instrumentation consists of x-ray and laser cameras mounted along the range to photograph the model in flight. For ablation testing, sphere-cone-cylinder nosetips with a nominal 0.05-in. nose radius and 45-deg cone half-angle were launched at 18,000 fps.

Figures 11 and 12 compare the nosetip shapes obtained from the photographic data to those predicted by the NOSEC code for tungsten and molybdenum tests, respectively. The boundary-layer transition and roughwall heating criteria that were used in the predictions are presented in Table 3. Scallop-augmented heating was used in the predictions because surface patterns that appear to be scallops were noted in some of the laser photographs of two tungsten shots, one at 200 torr and one at 325 torr.[4]

The tungsten test model was fired at a range pressure of 460 torr, yielding a stagnation pressure history from 210 atm at launch decaying to 140 atm at the last camera station. The

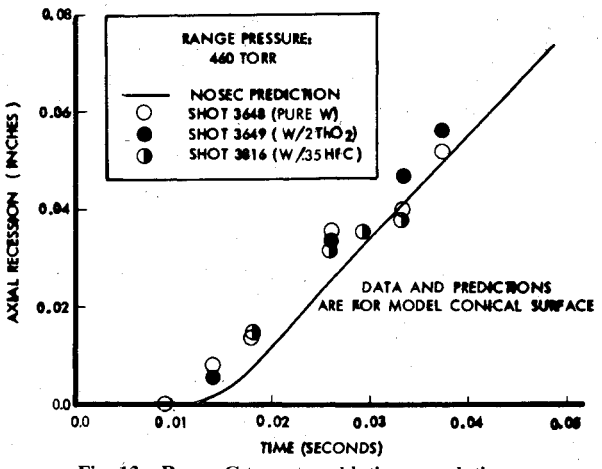

Fig. 13 Range G tungsten ablation correlations.

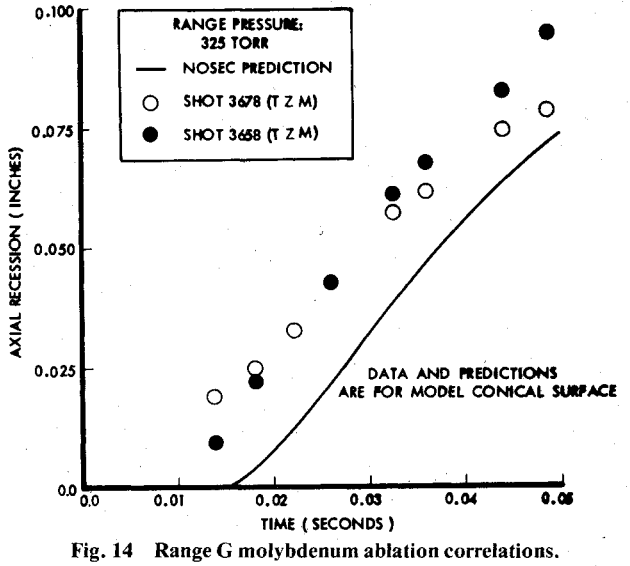

Fig. 14 Range G molybdenum ablation correlations.

molybdenum model was fired at 330 torr range pressure and experienced stagnation pressures from 150 atm to 120 atm. The necking down near the front of the cylindrical section is not due to an unusual heating distribution, but rather to the fact that the aft portion of the models is beryllium/copper.

Figures 13 and 14 compare the measured and predicted recession histories for the tests of Figs. 11 and 12, respectively, in addition to the data obtained, from other tests at the same conditions. The recession histories are for a point on the conical surface midway between the stagnation point and the cone-cylinder junction. It was felt that this location would provide a better check of the thermochemical ablation model, as recession there would be less influenced by two-dimensional conduction effects and shape change. It can be seen that the large melt resolidification collar that formed on the 50-Mw models does not appear in these tests, and that shapes and ablation rates are correlated very well.

IV. Sounding Rocket Tests

Two tungsten nosetips were flown on sounding rockets, one in clear air and the other in weather. In both cases, the nosetips were recovered intact. The initial contours and post-test photographs of the nosetips are presented in Figs. 15 and 16 for the clear air and weather flight tests, respectively. The band of solidified material starting midway aft on the cones is WO_3^* that has melted and run back. The lighter color downstream of the band is WO_3^* that formed at a temperature below its melt point. The differences in shape change and

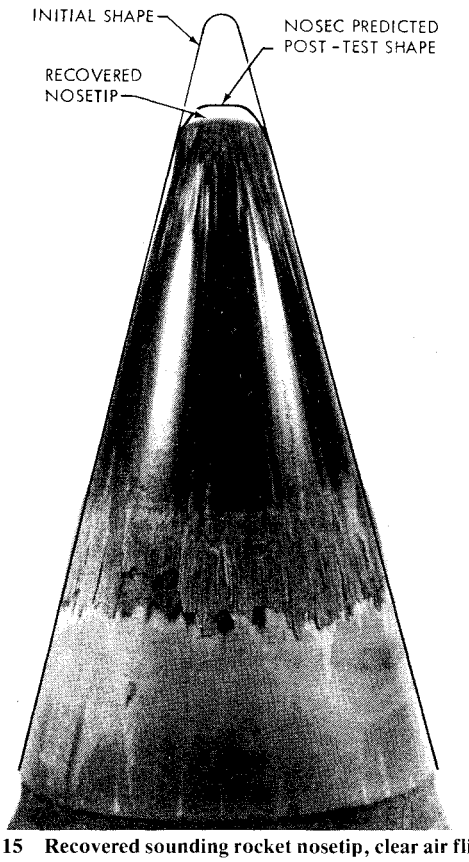

Fig. 15 Recovered sounding rocket nosetip, clear air flight.

total recession for the two nosetips are significant, even though the flight trajectories were essentially identical. The clear air nosetip, which showed no post-test evidence of surface scallop patterns, experienced a total axial recession of 0.401 in. The weather nosetip showed a significant amount of scallop patterns, and the total measured axial recession was 0.793 in.

The two flight tests have been analyzed using the NOSEC code with the transition and roughwall heating criteria presented in Table 3. The predicted post-test nosetip shapes are compared with the actual shapes in Figs. 15 and 16. The agreements between both predicted and actual shape change and total recession are excellent. The predicted total stagnation point recessions for the respective clear air and weather flights are within 9% and 1%, respectively, of the measured recessions. Particle erosion was included in the weather flight analysis, although the contribution of particle erosion to the total recession depth was predicted to be less than 1.0%. The weather particles are, however, believed to have initiated the formation of the surface scallop patterns. The augmented heating induced by the scallop patterns is predicted to be the mechanism causing the difference in clear air and weather recession.

V. Conclusions

Thermochemical ablation models have been developed for three refractory metals that are candidates for particle erosion-resistant nosetips. The models have been integrated into one- and two-dimensional ablation and conduction computer codes (the two-dimensional code also has shape change capabilities) and applied to ground and flight ablation tests. The correlations between predicted and measured recession and shape change were good, verifying the validity of the ablation models. In the application of the models to the ablation tests, it has been found that further investigations are required in the areas of 1) characteristic roughness height and its implication on boundary-layer transition and convective

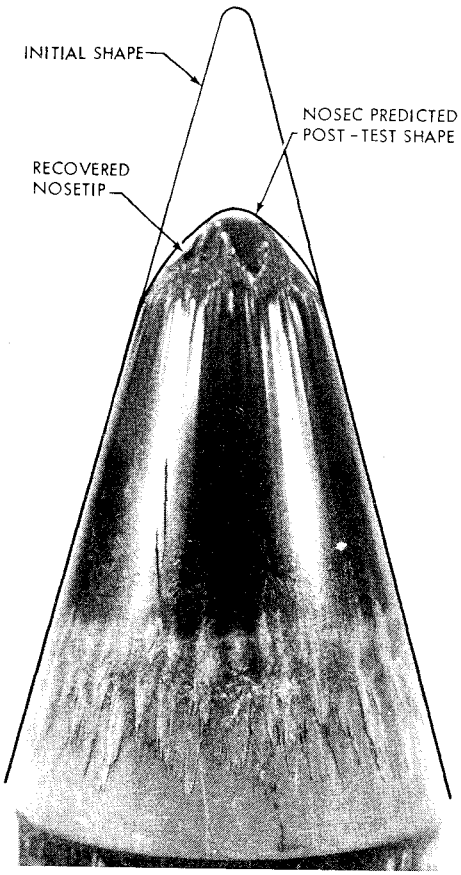

Fig. 16 Recovered sounding rocket nosetip, weather flight.

heating for refractory metal melt layers; 2) refractory metal stability criteria relative to the formation and growth of surface scallop patterns; and 3) liquid layer runoff and downstream resolidification.

References

[1]Sherman, M. M., "ANT/ERN Final Design Summary and Report,", Prototype Development Associates, Inc., Santa Ana, Calif., TR 1018-11-34, Nov. 1974.

[2]Moody, H. L, Sherman, M. M., Dunn, S. S., and Haddock, R. L., "The Development and Application of a Tungsten Ablation Model for Reentry Environments," Prototype Development Associates, Inc., Santa Ana, Calif., TR 1013-00-05, Jan. 1974.

[3]Dunn, S. S., "Tungsten Ablation Analysis for AFFDL 50 Megawatt Tests," Prototype Development Associates, Inc., Santa Ana, Calif., Private Communication (memorandum) to M. M. Sherman, March 1974.

[4]Smith, D. H., "Test Report for Aeroballistic Range Erosion-Resistant Nosetip (ERNT) Program," Prototype Development Associates, Inc., Santa Ana, Calif., TR 1018-15-12, June 1974.

[5]Moody, H. L., Smith, D. H., Haddock, R. L., and Dunn, S. S., "Tungsten and Molybdenum Ablation Modeling for Reentry Applications," AIAA Paper 75-112, Pasadena, Calif., Jan. 1975.

[6]Dension, M. R., "The Turbulent Boundary Layer on Chemically Active Ablating Surfaces," *Journal of Aerospace Sciences*, Vol. 28, June 1961, pp. 471–479.

[7]Gordon, S. and McBride, B. J., "Computer Program for Calculation of Complex Chemical Equilibrium Compositions, Rocket Performance, Incident and Reflected Shocks, and Chapman-Jouguet Detonations," NASA SP-273, 1971.

[8]Stull, D. R. and Prophet, H., *JANAF Thermochemical Tables*, National Bureau of Standards, Washington, D. C., Publication NSR-DS-NBS 37, June 1971.

[9]Perkins, R. A., Price, W. L, and Crooks, D. D., "Oxidation of Tungsten at Ultra-High Temperatures," Lockheed Missiles and Space Co., Sunnyvale, Calif., Rept. N63-18737, Nov. 1962.

[10]Arne, C. L., "Ablative Materials Subject to Combustion and Thermal Radiation Phenomena," Douglas Missile and Space Systems Division, Santa Monica, Calif., Paper 1851, Jan. 1964.

[11]Schick, H. L., *Thermodynamics of Certain Refractory Compounds*, Vol. II, Academic Press, New York, 1966.

[12]Margrave, J. L., "Thermodynamic Data for Selected Systems at High Temperatures," MAR CHEM, Inc, Houston, Tex., July 13, 1973.

[13]Powars, C. A., "Surface Roughness Effects on Reentry Heating," Aerotherm, Mountain View, Calif., TM-71-10, July 1971.

[14]Powars, C. A., "Analysis of PANT Series A Rough Wall Calorimeter Data," Aerotherm, Mountain View, Calif., Rept. 73-80, Sept. 1973.

[15]White, C. O. and Grabow, R. M., "Influence of Scallop Roughness on Nose Tip Shape Change Behavior," Philco-Ford Aeronutronic Division, Newport Beach, Calif., SAMSO TR 73-88, Jan. 1973.

[16]*Thermocphysical Properties Research Center Data Book*, Vol. 1, "Metallic Elements and Their Alloys," Purdue University, Lafayette, Ind., 1970.

[17]Smith, D. H., "Test Report: Segmented Stress-Resistant Tungsten Nosetip Test Program," Prototype Development Associates, Inc., Santa Ana, Calif., TM 1031-22-09, Jan. 1975.

[18]"The 50 Megawatt Facility of the Air Force Flight Dynamics Laboratory–Information for Users," Thermodynamics Branch, Flight Mechanics Division, Air Force Flight Dynamics Laboratory, Wright-Patterson Air Force Base, Ohio, TM 71-17FXE, Oct. 1971.